SPE 49299

A New Method for Saturation Measurements in Core Flooding Experiments

Johannes Bruining (SPE), Buu-Long Nguyen (SPE), Dietz Laboratory for Petroleum Engineering, and
Evert Slob, Dept. of Applied Geophysics, Centre for Technical Geoscience, Delft University of Technology

This paper was prepared for presentation at the 1998 SPE Annual Technical Conference and Exhibition held in New Orleans, Louisiana, 27–30 September 1998.

Abstract

In this paper we present an application of Frequency Domain Reflectometry (FDR) - an electromagnetic technique that measures the dielectric response of a transmission line. Such a response is related to the electric permittivity and conductivity distribution along the transmission line. In our experimental set-up the sample core replaces the dielectric material of a coaxial transmission line sample holder.

We use a recursive relation to derive the multiple reflection coefficient which is a function of the electric properties of the porous medium and thus a function of the water saturation.

We present an inverse modeling procedure which allows reconstruction of water saturation profiles from the measured multiple reflection coefficients. For the inverse modeling we use the Polak-Ribière conjugent gradient algorithm to extract the saturation distribution.

We show numerically and experimentally that the simulation profiles inclusive the position of the Buckley-Leverett shock front can be followed by a single measurement of the multiple reflection coefficient.

The results of our numerical experiments validate the inverse modeling procedure introduced in this paper.

Introduction

In most core-flooding experiments one measures flow rates and composition of injected and produced fluids without measuring saturations and composition within the core. Accurate determination of the relative permeability with the JBN method can be improved with a measured saturation distribution within the core including the capillary end effects. Existing method to measure saturations such as γ-ray attenuation however are experimentally tedious and expensive.

We show in this paper how the Frequency Domain Reflectometry (FDR) technique can be applied to measure the saturation distribution within rock cores during flooding experiments. The method is fast and cost effective. Next to the reconstruction of the saturation profile, the method can also be used to obtain calibration data of dielectric properties of fluid-saturated rock cores. Measurement of a complete profile takes typically a few minutes. However a central cable running through the core is required.

In the first section of this paper we give an expression for the multiple reflection coefficient as it is measured with the Frequency Domain Reflectometry (FDR) technique.

In the subsequent section, we present the numerical experiments which have been performed to validate the inverse modeling procedure. The forward modeling and inverse modeling procedures are described in detail in that section. We consider two methods (1) reconstruction of the saturation profile from a single measurement of the scatter function along the whole sample and (2) reconstruction of a single saturation profile by combining saturation profiles at various times.

We further describe the experimental setup used to measure the multiple reflection coefficient from a linear rock core during a displacement experiment, in which water is displacing oil. We apply the inverse modeling procedure to reconstruct the saturation profiles from the experimental data. The results of the numerical experiments and the core flooding experiments are described and discussed separately.

Appendix A presents the relationship between the water saturation and the electric properties of porous media.

Multiple Reflection Coefficient for a N-sectional Coaxial Transmission Line.

When an electromagnetic wave propagates along a transmission line with impedance discontinuities, multiple reflections will occur as the EM wave travels back and forth between the interfaces bounding domains of constant impedance. In our previous paper [1] we have derived the recurrent expression for the multiple reflection coefficient at the $(n\text{-}1)^{th}$ interface of a N-sectional coaxial transmission line,

i.e.

$$R_{n-1} = \frac{r_{n-1} - R_n \exp(-2\gamma_n l_n)}{r_{n-1} R_n \exp(-2\gamma_n l_n) - 1} \quad \ldots\ldots\ldots\ldots\ldots\ldots (1)$$

where l_n is the length of the n^{th} section, and

$$r_{n-1} = \frac{Z_{n-1} - Z_n}{Z_{n-1} + Z_n} \quad \ldots\ldots\ldots\ldots\ldots\ldots\ldots\ldots\ldots\ldots (2)$$

is the reflection coefficient due to change in impedance from Z_{n-1} to Z_n at the $(n-1)^{th}$ interface.

For a N-sectional coaxial transmission line, the multiple reflection coefficient at the $(N-1)^{th}$ interface is given by:

$$R_{N-1} = \frac{r_{N-1} - R_N \exp(-2\gamma_N l_N)}{r_{N-1} R_N \exp(-2\gamma_N l_N) - 1} \quad \ldots\ldots\ldots\ldots\ldots\ldots (3)$$

where R_{N-1}, r_{N-1}, γ_N and l_N are defined as above. R_N is the reflection coefficient at the end of the transmission line. Its value depends on how the transmission line is terminated. If the transmission line is open-ended in air or in a lossless medium, R_N = (1,0). When the transmission line is short-circuited, R_N will be (-1,0).

For a coaxial transmission line the impedance Z is related to the DC electric conductivity σ_{dc} [mho/m] and complex electric permittivity ε through the propagation coefficient γ [m^{-1}] as follows:

$$Z = \frac{i\omega\mu_0\mu \ln\left(\frac{b}{a}\right)}{2\pi\gamma} \quad \ldots\ldots\ldots\ldots\ldots\ldots\ldots\ldots\ldots\ldots (4)$$

where b is the inner radius of the outer conductor (shield) kept at zero potential (V=0) and a is the outer radius of the inner conductor; and

$$\gamma = \sqrt{i\omega\mu_0\mu\left(\sigma + i\omega\varepsilon_0\varepsilon\right)} \quad \ldots\ldots\ldots\ldots\ldots\ldots\ldots\ldots (5)$$

ε_0 is the electric permittivity of free space, μ_0 the permeability of free space. The permeability μ of the dielectric material filling the space between the shield and the inner conductor, is considered to be unity.

Numerical Experiments

Description of the Experiments. The numerical experiments described in this sections are intended to demonstrate and to validate the inverse modeling procedure, which enables to reconstruct the water saturation profile in a rock core from the FDR data.

The experiments are completed in two steps. In the forward modeling step, we generate the complex multiple reflection coefficient from a conceptual saturation profile. In the second step, we apply the inverse modeling procedure to reconstruct the given saturation profile from the generated complex multiple reflection coefficient.

We consider the inverse modeling techniques for two cases: 1) When we use a single measurement of the multiple reflection coefficient from a single saturation profile, and 2) When we use data of multiple measurements in a progressing saturation profile.

Forward Modeling Procedure. We model a case when water is displacing oil in a linear core. The core is originally filled with oil at connate water. The oil is displaced by water injected at one side and the fluids produced at the other. This means that we assume the Buckley Leverett saturation profile, with a gradually decreasing saturation upstream of a "shock" where the saturation steeply declines to the connate water saturation (Fig.1). The profile runs from the right (the injection side) to the left (the production side). Downstream of the shock the saturation remains constant and equal to the connate water saturation.

The length is taken to be 0.5m and terminates at 64/74 of the core length, where the core is cut. At that plane a very thin metal sieve is designed to be inserted to short circuit the transition line, providing R_N = (-1, 0).

Generating a water saturation profile. We simulate the water distribution by the Buckley Leverett model with capillary forces included in a horizontal tube.

$$\phi\frac{\partial S_w}{\partial t} + u\frac{\partial}{\partial x}\frac{\lambda_w}{\lambda_o + \lambda_w} = -\frac{\partial}{\partial x}\frac{\lambda_o\lambda_w}{\lambda_o + \lambda_w}\frac{dP_c}{dS_w}\frac{dS_w}{dx} \quad \ldots.. (6)$$

where λ_o and λ_w denote the phase mobility (ratio of permeability and viscosity) of oil and water, respectively. The boundary and initial conditions are:

S_w (x=0) = 1 – S_{or}
S_w (x, t=0) = S_{wc}
P_c (x=L) = 0

We use the Brooks-Corey model [4] for relative permeabilities and capillary pressure. Parameters are given in Table 1. The equations are solved with a third order Leonard scheme with a flux limiter [5].

In the first case, the Buckley-Leverett simulation is stopped at $t=t_1$=675s just before the shock reaches the starting point of the FDR probe.

In the second case, we include profile at $t=2t_1$=1350s and $t=3t_1$=2025s The saturation profile is to a good approximation a function of x/t (distance/time) only, except near the shock region. Note that this is also true for the dependent variables in many linear displacement processes in porous media.

Forward modeling the multiple reflection coefficient. The water saturation distribution in the core is modeled as a piece-wise constant profile. In other words we assume a number of sections in the core that each have a constant saturation. As we explain in App. A, the water saturation can be uniquely related to the complex electric permittivity and DC conductivity. Each section of the core possesses therefore a certain complex electric permittivity and DC conductivity. Hence the sample holder presents a number of coaxial slices with varying

impedance.

Such a variation in impedance results in multiple reflections that are defined by Eqs.1-3.

By short-circuiting the transmission line at the end of the measuring volume, we know R_N = (-1, 0). The advantage of this choice is that the termination of the transmission line is well defined. With R_N = (-1, 0) Eq.3 becomes:

$$R_{N-1} = -\frac{r_{N-1} + \exp(-2\gamma_N l_N)}{r_{N-1}\exp(-2\gamma_N l_N) + 1} \quad \ldots\ldots\ldots\ldots\ldots\ldots \quad (7)$$

If the saturation profile is known, the electric permittivity and conductivity and, subsequently, the propagation coefficient and the impedance of each slice of the core can be calculated using Eqs.A1-3 and Eqs.4-5. Substituting the values of impedance in Eqs.1-5&7 yields the complex multiple reflection coefficient at every interface.

The procedure is validated in [6] where we compare the results of the recursive reflection approach with the Green's function approach. The validity of the recursive reflection approach for coaxial transmission lines has also been proved in another work [1].

Using Eqs.A-1,2 & 3 and the simulated saturation profile, we calculate the electric permittivity ε and conductivity σ_{dc} for each section of the measuring volume. By substituting the values of ε and σ_{dc} in Eqs.5&4 we obtain the impedance of each section. The complex multiple reflection coefficient R_2 at the interface between the transition unit and the coaxial sample holder region can then be calculated using Eqs.1-5&7.

The simulated saturation profile for the first case at $t=t_1=675$s and $t=2t_1=1350$s is shown in Fig.1. The real and imaginary parts of the forward modeled complex reflection coefficients are shown in Fig.2&3. One clearly observes that the measured reflection coefficients for the two profiles are completely different.

Inverse Modeling Procedure. Here we describe the procedure of inverting back the saturation profile from the measured reflection coefficients.

The EM signal which travels along the transmission line is generated by a network analyzer. The latter also measures the S_{11} scatter function defined as ratio of the reflected power to the incident power [3]. The principle of *S*-parameter measurement is described in details in Ref.3.

Because we calibrate the network analyzer at the end of the cable, as it has been explained in our previous work [1], the measured S_{11} scatter function equals the multiple reflection coefficient at the interface between the cable and the transition unit.

The measured scatter function is thus a function of the dielectric properties and the geometric parameters of the transition unit and the sample holder.

As the geometric parameters and the dielectric properties of the transition unit are well known from the design, we can exactly model the phase shift and eventual energy loss due to this transition.

To facilitate our computations and optimization procedures, we correct the S_{11} scatter function for the transition unit, to obtain directly the multiple reflection coefficient at the interface between the transition unit and the measuring volume, which is defined by;

$$R_2 = \frac{S_{11} + r_{12}}{(S_{11}\, r_{12} + 1)\exp(-2\,\gamma_{tu}\, l_{tu})} \quad \ldots\ldots\ldots\ldots\ldots\ldots\ldots \quad (8)$$

where γ_{tu} and l_{tu} are the propagation coefficient and the length of the transition unit, respectively. The reflection coefficient r_{12} which occurs at the interface between the connecting cable and the transition unit is defined as

$$r_{12} = \frac{Z_1 - Z_2}{Z_1 + Z_2} \quad \ldots\ldots\ldots\ldots\ldots\ldots\ldots\ldots\ldots\ldots\ldots\ldots \quad (9)$$

where Z_1 and Z_2 are the impedance of the cable and the transition unit, respectively.

As this complex multiple reflection coefficient R_2 given by Eq.8 is related to the impedance and the propagation coefficient and hence to the water saturation, we can invert it to retrieve the saturation profile.

For this we define the target function which is the (frequency) sum of absolute values of the difference between the measured and computed (from an estimated saturation distribution) complex reflection coefficients. Note that in the numerical experiments considered in this section, the "measured" reflection coefficient is obtained from a forward computation of reflection coefficient from the saturation distribution divided in 64 steps. The optimal estimated saturation distribution minimizes the target function. For the minimization procedure we use the Polak-Ribière conjugent gradient method. The minimization procedure and the program used are described in [2].

Such an inversion algorithm does not usually lead to a unique solution and one needs to use all qualitative knowledge about the form of the saturation profile to obtain a good starting estimate. We distinguish between the situations:

A) The shock is within the measurement section of the tube.
B) The shock is outside the measurement section of the tube .

A. Shock is within the measurement section. For the first situation we need to take the position of the shock as a variable that is optimized in the minimization procedure. We start with a saturation value right (upstream of) the shock, which is slightly less than ($1-S_{or}$), where S_{or} is the residual oil saturation, and the connate water saturation left of the shock. We perform a forward computation of the target function by step wise (256 steps) increasing the shock position between 0 and 0.5 [m]. The starting point for the shock position is obtained where the target function is a minimum. With the thus obtained shock position and upstream saturation as an initial estimate (the down stream saturation remains equal to the connate water saturation) we apply the Polak-Ribière

algorithm to obtain the optimal values for the shock position and a single upstream water saturation. Now we divide the region upstream of the shock in two regions of equal length to which we assign as an initial estimate the single water saturation value obtained above. We apply again the Polak-Ribière algorithm to obtain the two optimal saturations upstream of the shock and the new optimal shock position. The saturation values downstream of the shock are left unchanged and equal to the connate water saturation. We continue to divide the upstream region now in four regions assigning the most upstream saturation value to the two upstream regions and the value just upstream of the shock to the two regions just upstream of the shock. We apply the Polak-Ribière algorithm to obtain the optimal four saturation values upstream of the shock and the best corresponding shock position. The saturation values downstream of the shock are left unchanged and equal to the connate water saturation. We continue the subdivision again by a factor two and repeat the procedure now to obtain the best eight saturation values upstream of the shock and the optimal shock position. Here we stop because a continuation of the procedure does not lead to new results (the saturation values remain unaltered in the procedure). For a longer core we expect that we can obtain 16 or more independent saturation values; for a shorter core we may have to stop at 4 or less independent saturation values upstream of the shock.

B. Shock is outside the measurement section. For the profiles which are obtained after the shock has moved outside the region which can be measured with the FDR probe we proceed as follows. First we determine single constant saturation value for which the target function is a minimum. This is the starting point for the next situation in which we divide the domain measured by the FDR probe in two equal regions with the same initial values of the constant saturation obtained above. We then determine two optimal saturations. We continue the procedure of dividing into two until no further improvement is obtained.

For the second case we combine the profiles at various times (here at 675,1350 and 2025 s) to construct a single profile. The profile with the shock is retrieved in the same way as described above.

Results and Discussion.

Case A: The result is shown in Fig.4. The drawn curve is the input. Buckley-Leverett saturation, which runs from the right (injection at x=0.584) to the left (production at x=0). The probe extends between zero and 0.5 m and does not reach the injection side at 0.584 m. In our set up the FDR probe does not reach so far as there may be an inhomogeneous fluid distribution at the injection side which makes the interpretation difficult. The dashed line shows two saturation values upstream of the shock. The dotted line shows four saturation values upstream of the shock and a slightly adjusted shock position. The final computation with eight saturation values is almost identical to the computation with four saturation values. The most upstream values are not obtained because the FDR probe does not reach so far. The agreement is, however, good. If this can also be achieved in practice FDR appears to be a inexpensive method to measure in situ saturation during laboratory experiments.

Case B: The result is shown in Fig.5. We observe that the retrieved saturation profile agrees very well with the original input profile.

Now we use the approximate model equation in which capillary forces are disregarded. In this case the theory predicts that the saturation is a function of the distance divided by time $S_w = S_w\left(\frac{x}{t}\right)$ Hence we rescale the distance that the saturation profile has traveled from the right at x= 0.578 m to the left by dividing this distance by the time. The situation is technically somewhat tedious because it is convenient to call the starting point of the FDR probe zero sothat the injection point at the right is at $\frac{length}{t_1} = \frac{0.578}{675} = 8.56e-4\left[\frac{m}{s}\right]$. The x-coordinate values are rescaled by subtracting the distance that the saturation profile has traveled from the right to the left divided by the time elapsed since injection was started. In summary we have done nothing else than rescaling the x-axis as *x/t*. The result is shown in Fig.6.

Experimental Measurements in Rock Cores

Features and Purpose. The experimental measurements described in this section are performed in an experimental setup which has been originally designed for the calibration measurement of dielectric properties of fluid-saturated porous media.

The FDR probe in this experimental setup has a length of only 10cm, which affects the relative resolution of the reconstructed saturation profile.

These experiments have therefore a preliminary character. The purpose is to verify whether we are able to reconstruct the water saturation profile from real measurement data, using the developed inverse modeling procedure.

Sample Holder. The main part of the experimental setup is the sample holder (Fig.7), part of which has a coaxial configuration. The sample holder is connected with a network analyzer by a standard 50Ω cable. To avoid additional reflections and to adapt the diameters of the cable and the coaxial cell we designed a cone-shaped transition unit with PTFE as dielectric material (Fig.7). Measurement of the impedance of the transition unit provided a value of 50.04Ω, which is adequate. The transition unit is located at the fluid outlet side of the sample holder and fully coincides with the end section of the sample. At the end of the transition unit, a copper sieve of 0.025mm thick is placed which should avoid the resonant cavity effects due to the specific form of the sample holder in the end section.

A stainless steel wire of 0.3cm diameter and 10cm length acts as the inner conductor. The sample section around the inner conductor is the measuring volume. A stainless steel cylinder of 3cm inner diameter acts as the outer conductor (shield). Note that this steel cylinder terminates at the sample point as the inner conductor. From that point it is prolonged by an acrylic tube to avoid uncontrollable energy losses of the EM signal. At the point where the inner conductor is terminated the coaxial transmission line is short circuited with a copper sieve of 0.025 mm thick. Because of the small thickness of the sieve, it would not affect the fluid flow.

At the beginning and the end of the measuring volume pressure transmission units with semi-permeable (hydrophillic and hydrophobic) membranes are installed. This enables measurement of pressure drop in every fluid phase (water, oil) and measurement of capillary pressure across the core at these points. Water and/or oil are injected into the sample holder from the right and are produced at the left.

Sample configuration. In order to reduce the effects of injection inhomogeneities at the inlet side and the capillary end effects, the sample is constituted from three sections. The entrance section between the inlet chamber and the copper sieve, the measuring section along the inner connector and the end section which coincides with the transition unit.

Materials.

Fluids. We use water with an electric conductivity of 7.9×10^{-4} mho/m. A mineral oil containing surface active compounds is used to model the oil phase.

Rock cores In all experiments described in this paper we use the Bentheimer sandstone because. This sandstone is the reservoir sandstone of the Schoonebeek oil field, the largest on-shore oil field in North West Europe. Furthermore it also forms a reservoir for all the oil and gas fields west of the river Ems in Germany, the Emsland region (Emlichhem, Scheerhorn, Ruhle, Rhulemoor, etc.). The sandstone has a porosity of about 25% and a permeability ranging from 500 to 10,000 mD. The samples used in our experiments have a permeability of about 2300mD. The grain diameter varies from 0.1 to 0.3mm and is classified as a fine to medium sandstone.

The Bentheimer sandstone consists of mainly quartz. There are however some other minerals present. Mineralogical and scanning electron-microscopic (SEM) investigations show the presence of clay minerals like kaolinite and illite which are formed as results of diagenetic conversion of feldspars. Quartz overgrowth is also observed. Any cement of the sandstone being present exists of chalk that is mostly dolomitized. Furthermore, there is also a small amount of iron present in the form of siderite that sometimes forms crusts of iron oxide. The iron if present can have a cementing function.

The method introduced in this paper requires a central conductor running through the sample. This configuration can cause spurious flow problems. We expect, however, that such problems can be solved e.g. by the application of molten metal or other techniques.

Establishing Calibration Parameters. As we explain in App. A, the reconstruction of the saturation profile requires the knowledge of electric permittivity of the components constituting the porous media, i.e. the rock matrix, the water and the oil. The electric permittivity of rock, oil and water can be obtained by inverting the reflection coefficients measured in those media [1]. For measurements in fluids, the sample holder is held vertical and filled with the fluid up to the end of the inner connector. The transmission line is also short-circuited at that point.

First we use the FDR probe to perform a reflection measurements in a measuring cylinder filled with the water and oil used in the experiment. Then we measure the reflection coefficient for the dry rock core. From the measured complex reflection coefficients we calculate the propagation coefficient $\gamma(\omega)$. We establish the real and imaginary parts ε' and ε'' of the complex electric permittivity of the fluids and the dry rock.

We continue to perform measurements on a core. The core is first vacuumed and subsequently saturated with water at extremely low flow rate. Under such conditions it is reasonable to assume that the core is fully filled with water i.e. $S_w = 1.0$. We measure the reflection coefficient in the core. We establish the real and imaginary parts ε' and ε'' of the complex electric permittivity.

Subsequently we inject oil through the core with gradually increasing injection rate to displace water for 24 hours. We then assume that the core is uniformly filled with oil at connate water saturation $S_w = S_{wc}$ and $S_o = 1 - S_{wc}$. In other words we assume that fluctuations in the saturation distribution are small with respect to the wave length of the EM radiation. Again we measure the reflection coefficient in the core and calculate the propagation coefficient. From the latter we establish the real and imaginary parts ε' and ε'' of the complex electric permittivity. Subsequently we displace the oil with water at a Darcy velocity of 1.04e-5m/s. We perform totally 26 measurements of the reflection coefficients. The time interval between two measurements is 3min.

After finishing the measurement series, we continue to inject water at a high rate for 24 hours. We assume that after this no movable oil remains in the core and the core has reached residual oil saturation S_w=1–S_{or}. We then perform the last measurement of the reflection coefficient.

We interpret the measurements in terms of a complex electric permittivity $\varepsilon^* = \varepsilon' - i\,\varepsilon''$. For this complex electric permittivity we assume that the complex refractive index model (Eq.A-2) applies. The component electric permittivites ε^*_{water} and ε^*_{oil} are determined by the measurement in the pure fluids. For the frequency range we use in our measurements, the real and imaginary parts of the complex electric permittivity appear to be constant. The complex electric permittivity of rock and the exponent α of the mixing rule (Eq.A-2) are determined from the best fit of the experiments at connate water saturation, residual oil saturation and at water saturation S_w = 1. The thus obtained parameters for water, oil and dry rock are summarized in Table 2. The exponent of the mixing rule has been found to be 0.45.

Simulating Saturation Profiles with Inverse Modeling. In order to reconstruct the saturation profiles within the sandstone core during the experiments, we apply the inverse modeling procedure which has been described and validated above in the numerical experiment for case A (single measurement on single profile with shock).

Results and Discussion. Figure 8 shows the saturation profiles, reconstructed from the FDR measurements of reflection coefficients at various times, versus distance from the beginning of the measuring volume. Here we show only the reconstructed profiles at t = 888, 1459, 2404 and 3766s. In all cases, the position of the shock has been determined. The figure also shows the movement of the shock in time.

The limited length (0.104m) of the FDR probe we use in these experimental measurements does affect however the relative resolution of the reconstructed saturation profile. Note that for t=888s, we could obtain only one independent saturation value upstream the shock. At t=1459s and t=2404s two independent saturation values are distinguished upstream the shock. At t=3766s, we observe a number of saturation steps in the profile. Indeed also here the limited extent of the measuring volume does not allow for a more detailed going interpretation than four independent saturation values upstream of the front.

We also show in this figure the saturation profile, reconstructed from measurement data for the fully water-saturated core. The resolution problem is clear.

We expect that increasing the probe length will provide better results with higher resolution.

At this moment we are working on the design of a new sample holder for long rock cores.

Conclusions

1. We have shown both theoretically and experimentally that the Buckley-Leverett shock-front can be followed by a single FDR measurement of the multiple reflection coefficient.

2. The numerical experiment validates the procedure of reconstructing the saturation profile from a single measurement of the multiple reflection coefficient.

3. By combining the profiles at various times, we can reconstruct a single saturation profile which agrees very well with the original input profile.

4. Model equations are often used to interpret core flooding experiments in terms of constitutive parameters e.g. the relative oil and water permeability. FDR can be used to improve interpretation with these methods.

Acknowledgments

We thank Delft U. of Technology and Shell International BV for the financial support.

We thank the technical staff of the Dietz Laboratory for Petroleum Engineering, especially Henk van Asten, Peter de Vrede, André Hoving and Léo Vogt for their assistance in the design, construction and maintenance of the experimental setup. Thanks are extended to Karel Heller, Marcel van den Broek en Ton Van Leeuwen for their indispensable help in data acquisition

References

1. Nguyen, B-L., Geels, A.M., Bruining, J. & Slob E.C.: "Calibration Measurements of Dielectric Properties of porous Media", *SPE paper No. 38715, Proc. of the 1997 SPE Annual Technical Conference and Exhibition held in San Antonio, Texas,* 5-8 October, **Ω-II**, 13-21.
2. Press, W.H., Teukolsky, S.A., Vetterling, W.T. and Flannery, B.P.: *Numerical Resipes in C: the Art of Scientific Computing*, 2d Edition, Cambridge U. Press (1992).
3. Hewlett Packard: HP8753A Network Analyzer - System Operating and Programming Manual.
4. Gupta, A.D., Lake, L.W., Pope, G.A. and Sepehrnori, K.: "High Resolution Monotonic Schemes for Reservoir Fluid Flow Simulation", *In Situ*, 15(3), 1991, 289-317.
5. Brooks, R.H., Corey, A.T.: *Hydraulic Properties of porous Media*, Colorado State Univ., Fort Collins, Colo., Hydrol. pap. No.3, 1964.
6. Nguyen, B-L, Bruining, J, Slob, E.C. and Hopman, V.: "Delineation of Capillary Transition Zone from Ground Penetrating Radar Data", *SPE paper No. 36638, Proc. of the 1996 SPE Annual Technical Conference and Exhibition held in Denver, Colorado,* 6-9 October, **Π**, 647-660.

Appendix A. Relationships between Water Saturation and Electric Properties of Fluid-Saturated Porous Media

As the impedance $Z(\omega)$ can be expressed in terms of the propagation coefficient $\gamma(\omega)$ (Eq.4). Eq.1 can be inverted for each frequency ω to obtain $\gamma(\omega)$. The purpose of this Appendix is to give a procedure to relate the propagation coefficient $\gamma = \sqrt{i\omega\mu_0\mu\left(\sigma + i\omega\varepsilon_0\varepsilon\right)}$ to the water saturation.

For this we use well established empirical relations.

The conductivity σ is estimated form Archie's second law

$$\sigma = \phi^m S_w^n \sigma_w \quad \text{..... (A-1)}$$

where *m* and *n* are the Archie's exponents to be determined from the experiments described above and σ_w is the electric conductivity of water.

We use the complex refractive index model (CRIM) which presents a simple power (α) law weighted average of the constituent dielectric permittivity to obtain the effective dielectric permittivity ε_m of the porous medium

$$\varepsilon_m^\alpha = (1-\phi)\varepsilon_{rock}^\alpha(\omega) + \phi S_w \varepsilon_w^\alpha(\omega) + \phi(1-S_w)\varepsilon_{oil}^\alpha(\omega) \text{ .. (A-2)}$$

where the frequency dependence of component complex electric permittivity are given by the Debye's equation:

$$\varepsilon_k^*(\omega) = \left(\varepsilon_{k,\infty} + \frac{\varepsilon_{k,s} - \varepsilon_{k,\infty}}{1 + (i\omega/\omega_{k,rel})} \right) - \frac{i\sigma_{k,dc}}{\omega\varepsilon_0} \quad \text{..... (A-3)}$$

where ε_s, ε_∞ are static and infinite (apparent) dielectric permittivities, respectively; ω_{rel} is the relaxation frequency and ε_o is the dielectric permittivity of free space The subscript *k* denotes rock, water or oil.

The effective dielectric constant ε_m as described by Eq.A-2 and Eq.A-3 is a function of the saturation only as all other parameters can be determined in separate experiments.

Substituting Eqs.A1-3 in Eq.5 yields a relationship between water saturation and the propagation coefficient $\gamma(\omega)$.

Table 1. Parameters used in forward modeling of the multiple reflection coefficient

Quantity	symbol	value	unit
Archie exponent for porosity	m	1.5	[-]
Archie exponent for saturation	n	2.0	[-]
relative end point permeability of oil	k'_{ro}	1.0	[-]
relative end point permeability of water	k'_{rw}	0.5	[-]
connate water saturation	S_{wc}	0.15	[-]
residual oil saturation	S_{or}	0.20	[-]
impedance of the cable and the transition unit	$Z_1=Z_2$	51	[Ω]
exponent for the dielectric mixing rule	α	0.5	[-]
static dielectric constant of oil	$\varepsilon_{oil,s}$	1.991	[-]
static dielectric constant of rock	$\varepsilon_{rock,s}$	4.5	[-]
static dielectric constant of water	$\varepsilon_{w,s}$	78.36	[-]
dielectric constant of water at high frequency	$\varepsilon_{w,\infty}$	1.776	[-]
dielectric constant of oil at high frequency	$\varepsilon_{oil,\infty}$	1.989	[-]
dielectric constant of rock at high frequency	$\varepsilon_{rock,\infty}$	4.5	[-]
oil viscosity	μ_o	8e-3	Pa.s
water viscosity	μ_w	1e-3	Pa.s
Corey exponent	γ	3	[-]
relaxation frequency of oil	$\omega_{oil,\,rel}$	1e15	[s^{-1}]
relaxation frequency of rock	$\omega_{rock,\,rel}$	1e15	[s^{-1}]
relaxation frequency of water	$\omega_{w,\,rel}$	1e10	[s^{-1}]

Table 2. Real and imaginary parts of complex electric permittivity of water, oil and rock used in the experiments.

Material	Real part of ε^*	Imaginary part of ε^*
Water	81.79	4.93
Oil	2.16	0.022
Rock	4.28	0.21

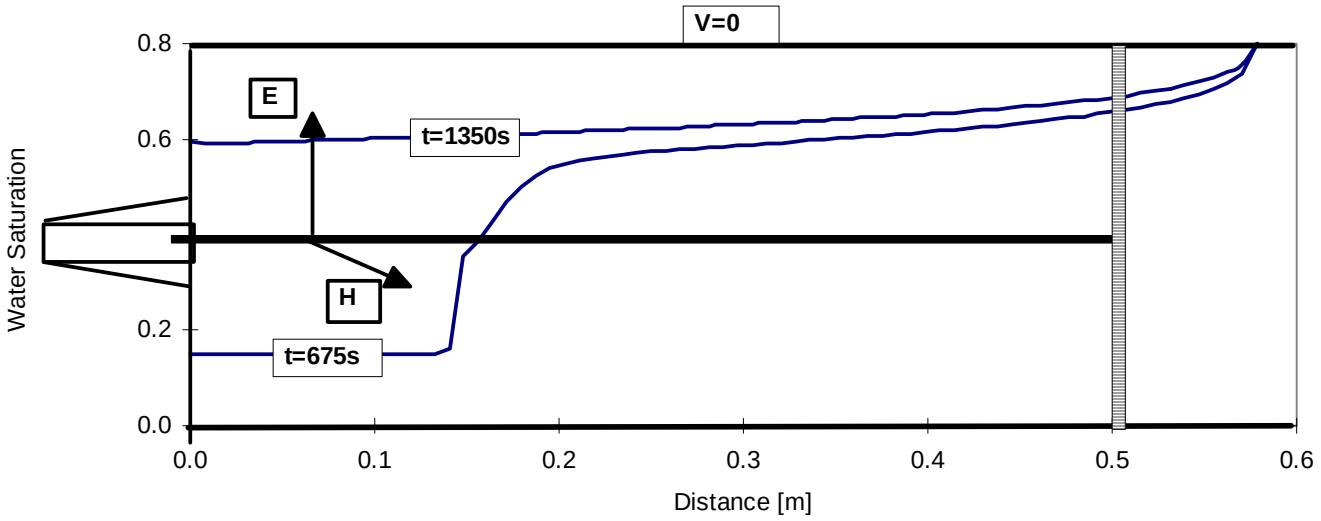

Figure 1. Measurement of profiles at t=675s and t=1350s

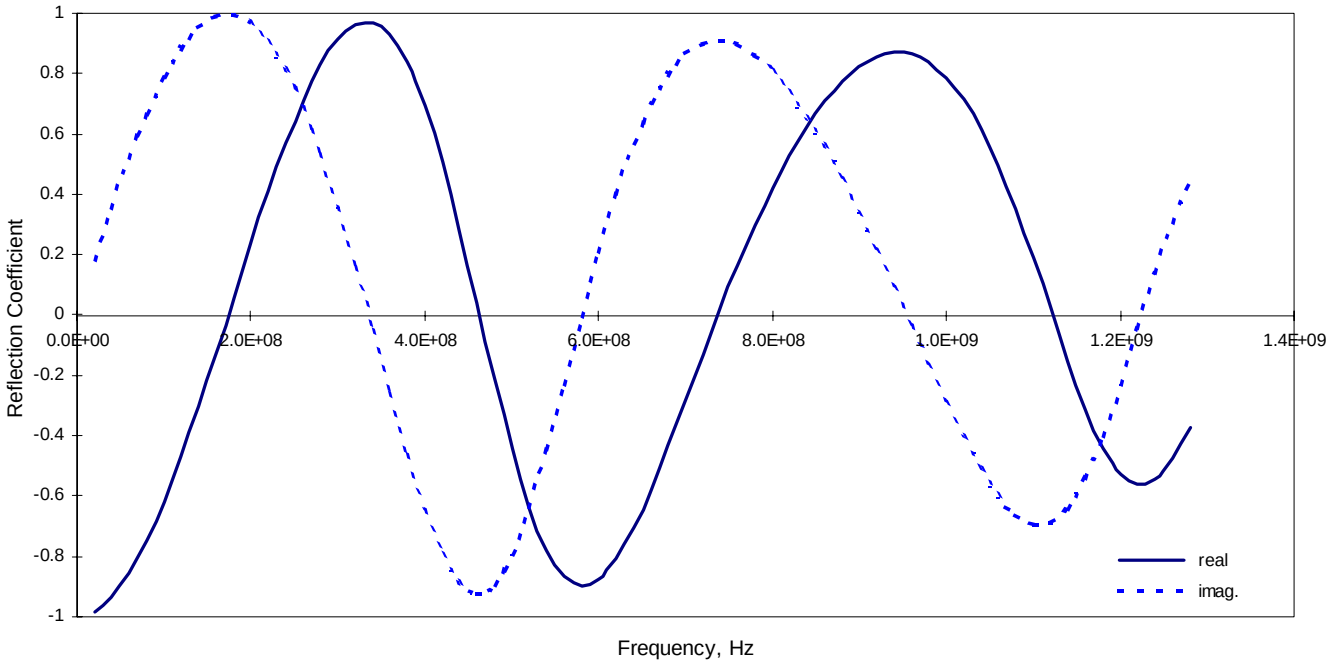

Figure 2. Multiple reflection coefficients at the transition unit/measuring volume interface measured at t=675s

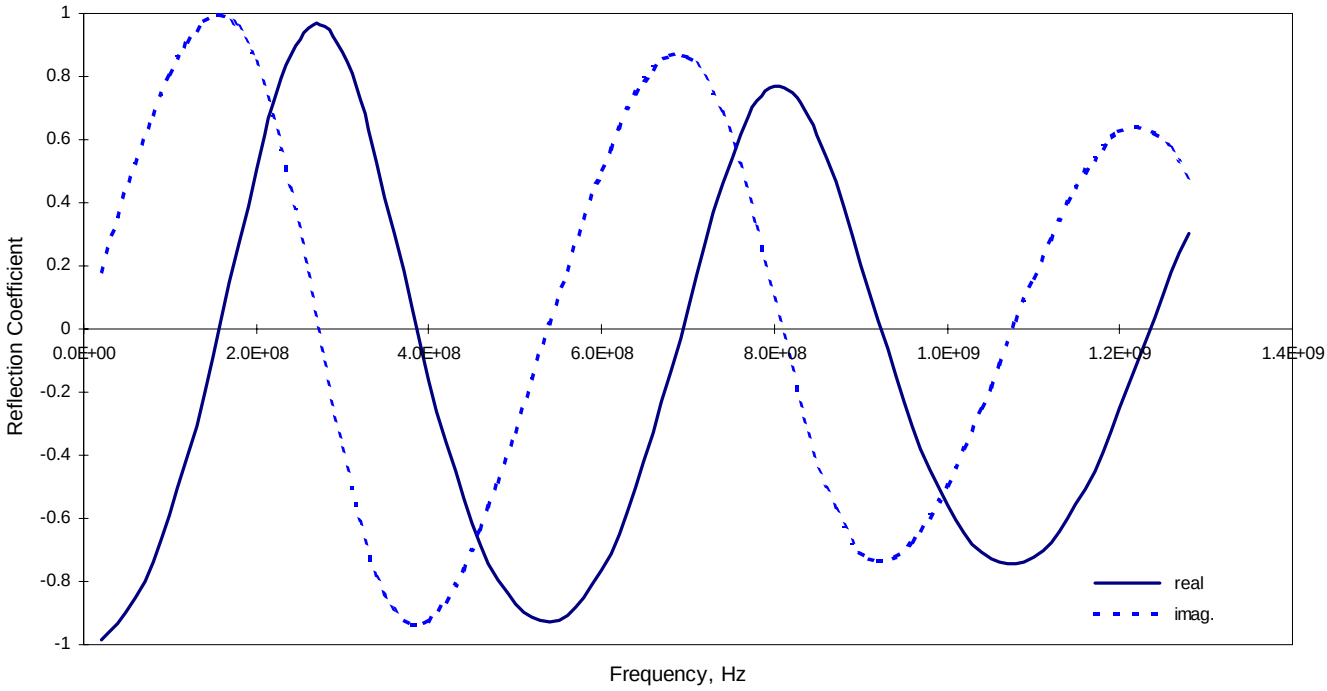

Figure 3 Multiple reflection coefficients at the transition unit/measuring volume interface measured at t=1350s

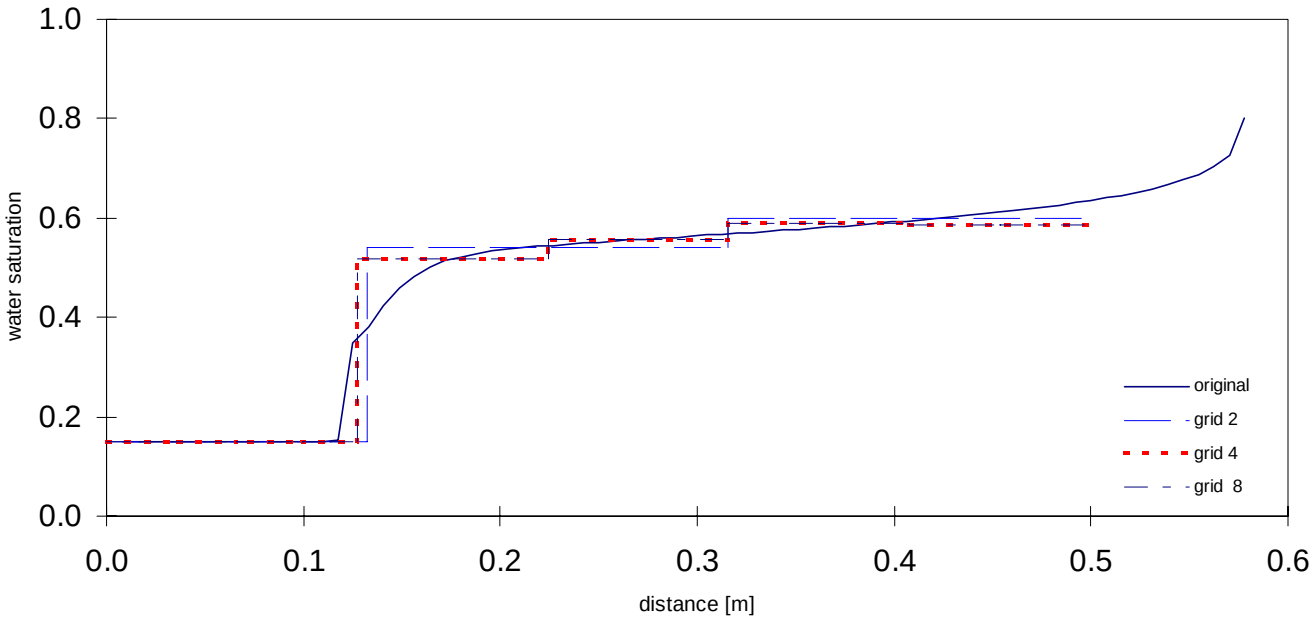

Figure 4. Original input and inversely reconstructed single water saturation profile

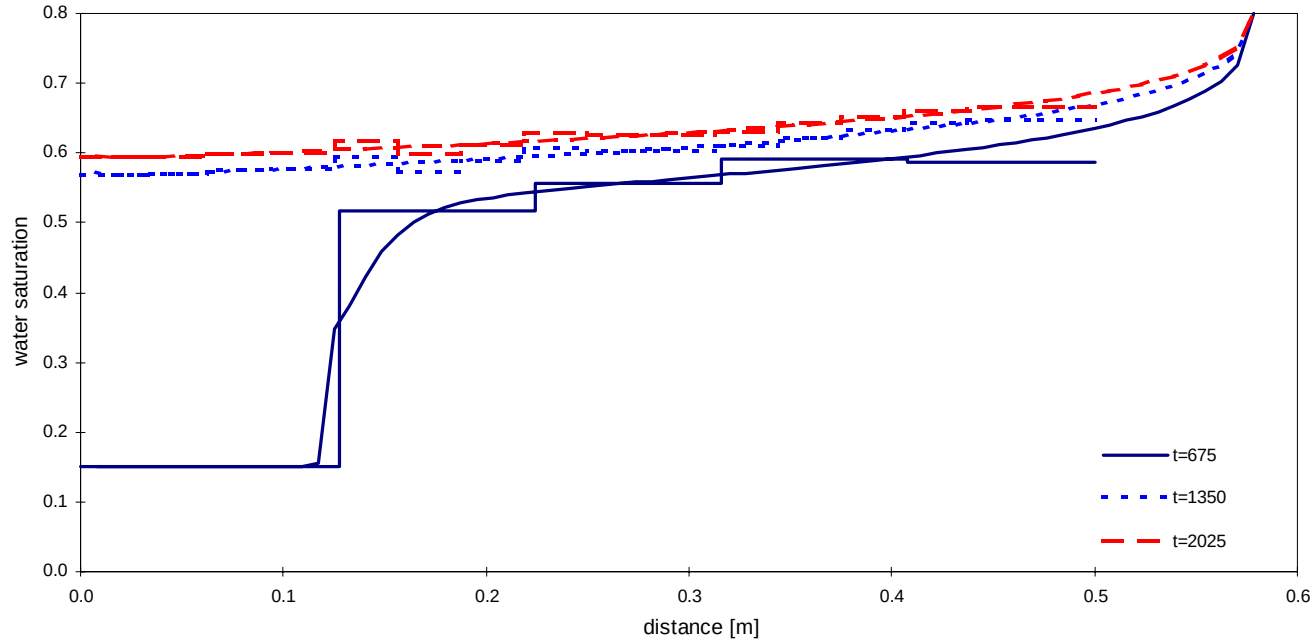

Figure 5. Input and inversely reconstructed water saturation profiles (case B)

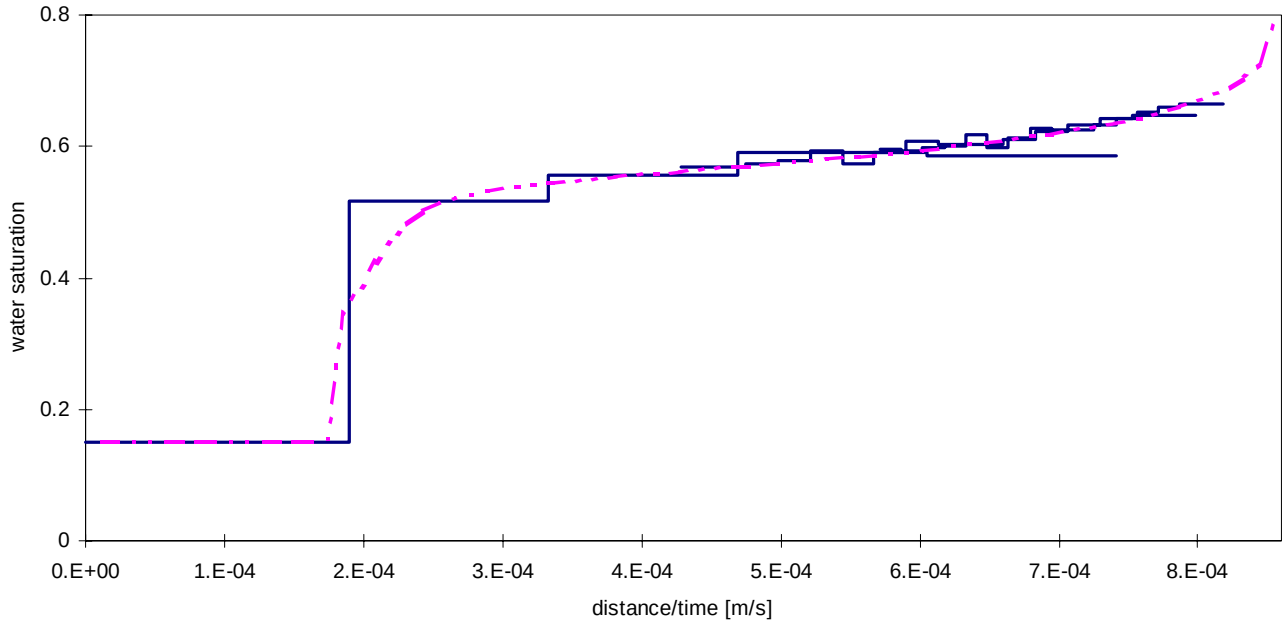

Figure 6. Water saturation versus x/t

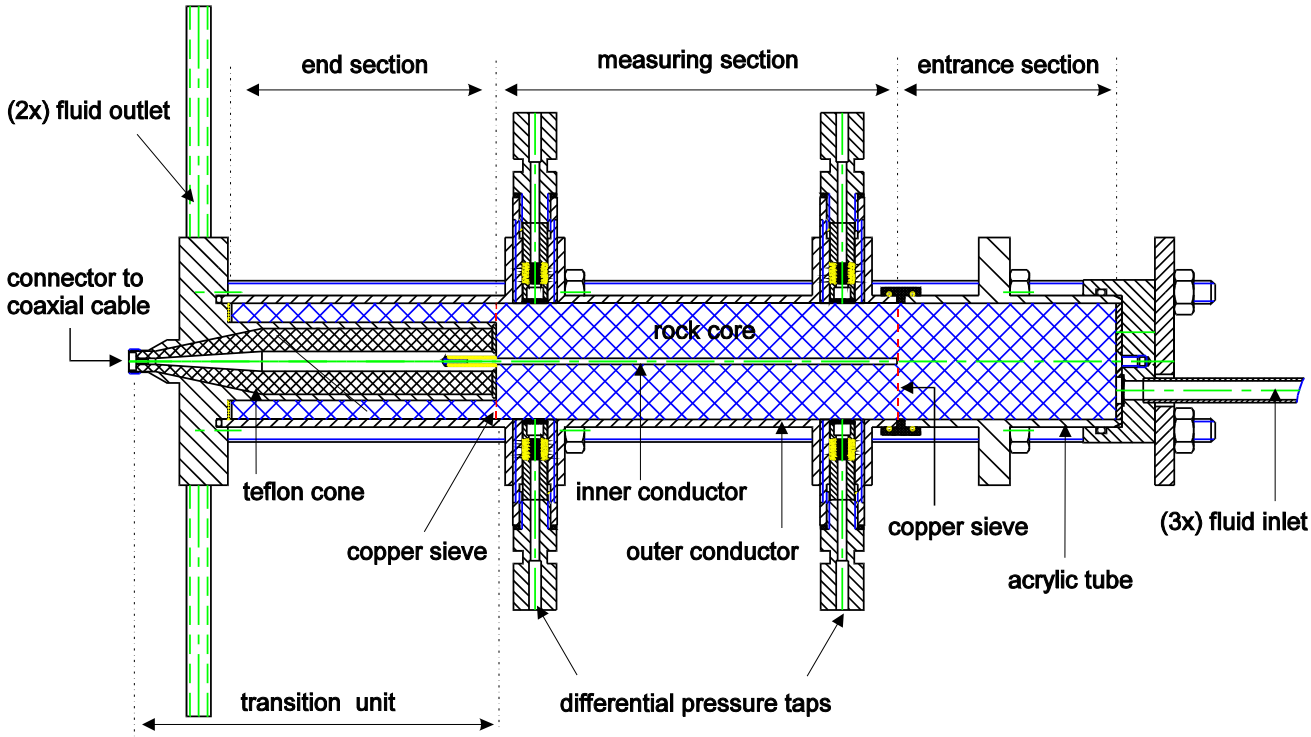

Figure 7. Technical drawing of the coaxial sample holder

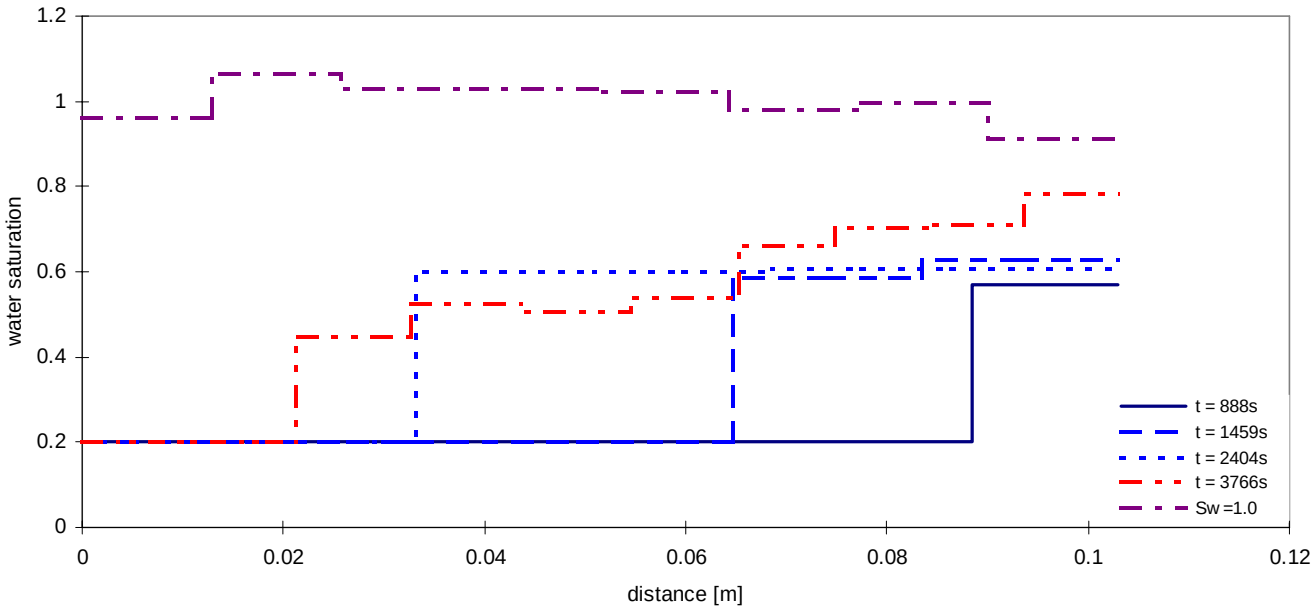

Figure 8. Water saturation profiles inversely reconstructed from experimental data